Research article

The Ballina soft soil Field Testing Facility

Jubert A. Pineda[1,*], Richard B. Kelly[1,2], Laxmi Suwal[1], Lachlan Bates[1] and Scott W. Sloan[1]

[1] Priority Research Centre for Geotechnical Science and Engineering, School of Engineering, The University of Newcastle, Callaghan Campus, Newcastle, 2300, Australia
[2] Snowy Mountains Engineering Corporation, SMEC, Australia

* **Correspondence:** Email: jubert.pineda@newcastle.edu.au; Tel: +6102497034.

Abstract: An overview of the work done at the Ballina soft soil Field Testing Facility (NFTF), established near the town of Ballina (New South Wales, Australia) by the ARC Centre of Excellence for Geotechnical Science and Engineering (CGSE), is presented in this paper. The testing facility is aimed at carrying out fundamental research for providing solutions to problems associated with energy and transport infrastructure in Australia. Development of the field testing facility was driven by challenges with soft soil engineering at the nearby Ballina Bypass motorway project. The state road authority, the contractor and the designers helped to create the concept which was fleshed out and delivered by the CGSE. The main outcomes of comprehensive *in situ* and laboratory characterization studies are presented and discussed. Results of experimental studies carried out by the CGSE to assess sampling disturbance in the soft soil deposits encountered at the Ballina site are also presented. Last but not least, the paper discusses the main findings and lessons learnt from an international symposium organized by the CGSE in 2016 to assess current practice for predicting the behaviour of embankments constructed on soft soils.

Keywords: soft clay; estuarine clay; Sherbrooke sampling; sampling disturbance; *in situ* tests; advanced laboratory testing; embankment behaviour

1. Introduction

Soils are inherently variable due to the nature of their deposition. Natural soft soils are typically weakly cemented and highly compressible. These features increase the likelihood of failure of civil engineering infrastructure built on them. Even if failure is not of concern, large settlements may occur during and after construction due to their high compressibility. These excessive settlements

can deform geotechnical structures increasing the cost of maintenance. The challenges encountered with soft soil engineering at the Ballina Bypass motorway project (New South Wales, Australia), motivated the Ballina Bypass Alliance (RMS, Leighton Contractors, AECOM, SMEC and Coffey) to generate a legacy initiative where land acquired for the bypass could be used as a National Field Testing Facility (NFTF). The idea was taken up by the ARC Centre of Excellence for Geotechnical Science and Engineering (CGSE) who established the new facility near the town of Ballina, in northern New South Wales, and performed a comprehensive site characterisation study to quantify material behaviour. The facility has been successfully used to perform high-quality research with the aim of giving solutions to problems associated with energy and transport infrastructure in Australia.

This paper provides an overview of the work done at the NFTF over the last five years. The main results obtained from *in situ* and laboratory characterization studies [1,2] are combined in this paper with the results of a microstructural study carried out to assess the effects of tube sampling on soil fabric [3]. In addition, the main outcomes of an international prediction symposium held in Newcastle in 2016, which focused on predicting the behaviour of a trial embankment constructed on soft soil [4], are presented and discussed. The paper closes discussing the lessons learnt from the work carried out and the legacy provided by the Field Testing Facility to the local roads authorities, local and international practitioners and academics.

2. Location, site geology and geomorphology

The site is located to the northwest of Ballina and occupies 6.5 Ha of land. Figure 1a shows the regional geological setting at Ballina site. A plan view of the testing facility is presented in Figure 1b,c which include the location of *in situ* tests and boreholes drilled to obtain tube and block specimens for laboratory testing. The ground surface is located at 0.5 m Australian Height Datum (AHD). It reduces slightly to about 0.3 m AHD at the northern and eastern sides of the site adjacent to Emigrant and Fishery creeks respectively. A 1.5 m thick access track was constructed along the western boundary prior to performing the site characterisation. As observed in Figure 1b, geotechnical infrastructure constructed over the last five years at the NFTF comprises two rectangular embankments (PVD and No PVD), one circular embankment (Vacuum) as well as four shallow footings.

The adjacent hillsides to the NFTF are comprised of basalt rock overlying argillite. A tuffaceous clay layer occasionally occurs between the basalt and the argillite. The basalt has been weathered to residual soil in its upper horizon. The weathering sequence comprises aluminium, magnesium and iron montmorillonite, then poorly crystalline montmorillonite and finally kaolinite/halloysite. Interstratified illite/smectite may be formed if potassium is present. The formation of clay minerals is favoured by the relatively high temperature in the area. The high rainfall in the Ballina region and the permeable nature of the basalt rock have promoted an extensive and rapid leaching of minerals [5]. This explains the high proportion of clay particles and the dominant clay minerals (e.g., illite, kaolinite and smectite) of the natural sediments at the NFTF.

Bishop [6] identified quaternary deposition sequences for deposits in the Richmond River valley. The first deposition (Pleistocene Age) comprised 1 m to 2 m thick deposits of fluvial sandy gravels overlaid by very stiff oxidised clays. These deposits have been eroded and exist generally from bedrock to RL-15 m AHD. A Palaeochannel, eroded through the stiff clay deposits, is located to the east of the NFTF below the Fishery creek. The sequence is completed by the Holocene Age

sediments that infilled the Richmond River estuary as a consequence of the rise in sea level. These sediments vary from gravels and sandy clays at lower levels to shelly muds in the upper levels. Soils above RL-10 m AHD are typically clays. The presence of interbedded estuarine sands and muds below RL-10 m AHD suggests that soil deposition occurred upon high energy conditions (i.e. under fast-moving water) [6]. On the other hand, the absence of sands above RL-10 m AHD seems to coincide with the formation of a coastal barrier that produced a low energy estuarine depositional environment behind it between 8000 and 9000 years BP.
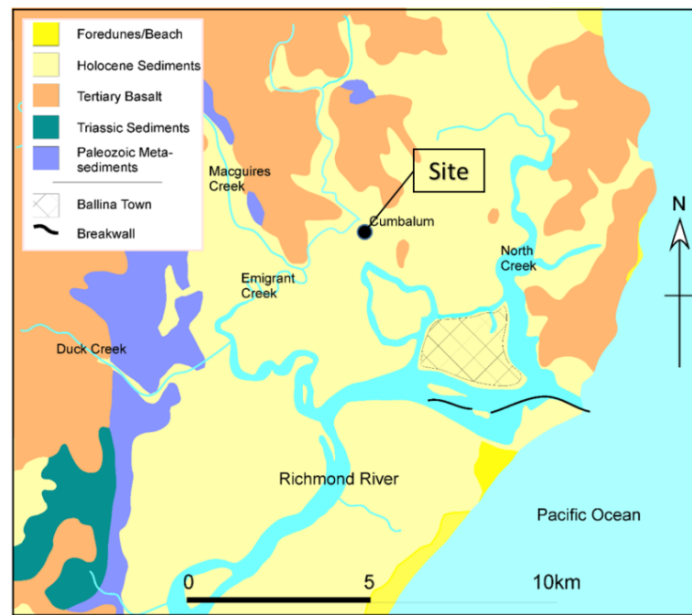
(a)
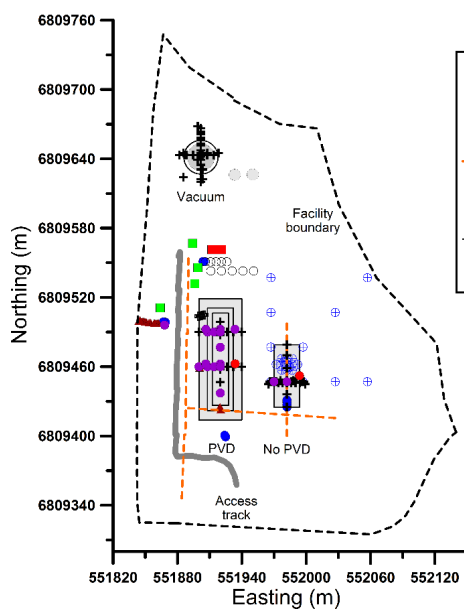
(b)
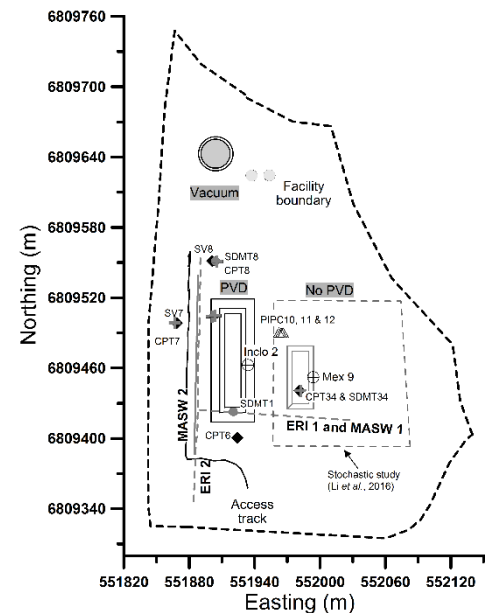
(c)

Figure 1. Ballina site (NFTF). (a) Geological setting (after [6]). (b) Plan view. (c) Plan view and location of in situ tests.

Differences in sedimentation rates across the fluvial delta seems to indicate that the estuary was infilled in a highly heterogeneous process. The location of the NFTF appears to be sufficiently distant from the coastal barrier that the sediments would have been mostly deposited under water. This interpretation is supported by the lack of sand lenses within the estuarine clay. Oedometer test results reported by Bishop and Fityus [7] indicated that the clays above 4 m depth were deposited in a tidal flat environment while clays below 4 m depth were formed in the less dynamic deeper water environment. The last stage of deposition in the area is associated with flooding which occurred since the sea level has fallen. These sediments are composed of sands, silts and clays. Whereas the soil deposits encountered at the NFTF are likely to be geologically normally consolidated, overconsolidation through seasonal changes in groundwater levels, creep or thixotropy may have occurred.

3. Soil composition, mineralogy and fabric

Mineralogical analysis (XRD) performed on soil specimens obtained at different depths within the soil profile (Figure 2a) shows that specimens are composed of: amorphous minerals, kaolinite, illite, quartz, interstratified illite/smectite, plagioclase, pyrite, K-feldspar, mica and calcite. An average organic content of 3% is presented in the soil deposits located below 4 m depth. As observed in Figure 2b sodium (0.93–8.23 g/L) and chloride (2.5–15.4 g/L) are the most abundant cations and anions in the pore fluid. The alkalinity of the pore water lies between 0.6 and 2.2 g/L of $CaCO_3$.

The variation with depth of the electrical conductivity of the pore fluid, EC_{fluid}, and bulk material, EC_{bulk}, is shown in Figure 2c. EC_{bulk} increases with depth from 4 mS/cm to 15 mS/cm. The reduction in EC_{bulk} at 11.1 m depth indicates a change in soil composition. EC_{fluid} varies from 7 mS/cm up to 36 mS/cm (the average below 5 m). The important salt concentration during the deposition of these sediments tends to form a loose porous fabric composed by large and dense aggregates separated by large voids. This explains the large void ratios estimated for the natural clay as discussed below (~3).

Scanning Electron Microscopy (SEM) and Mercury Intrusion Porosimetry (MIP) analyses, were used to evaluate the microstructure (fabric) of Ballina clay. SEM images obtained on high-quality block specimens retrieved with the Sherbrooke sampler are compared in Figures 3 and 4 against the fabric of the reconstituted clay (one-dimensionally consolidated under 70 kPa). Before MIP and SEM testing, specimens were pre-treated using the so-called freeze-drying technique [8] in order to minimize changes in soil structure. Figure 3 indicates that both natural and reconstituted clay show an open fabric with predominant macro pores of around 1 μm. Fabric anisotropy is not evident for the natural Ballina clay specimen. Pore size density (PSD) functions were obtained from MIP tests. The PSD was estimated from the derivative of the cumulative intrusion curve according to:

$$f(\log x_m) = -\frac{\delta(e_{MIP})}{\delta(\log d)} \qquad (1)$$

where $\log(x_m)$ is the midpoint of the pore diameter class. The comparison of the PSD curves confirm the predominance of macro pores of around 1 μm. However, the peak density value for the natural clay is significantly higher. This indicates similar structural arrangement for natural and reconstituted specimens. The main difference lies in the fact that the natural soil has larger numbers of pores with
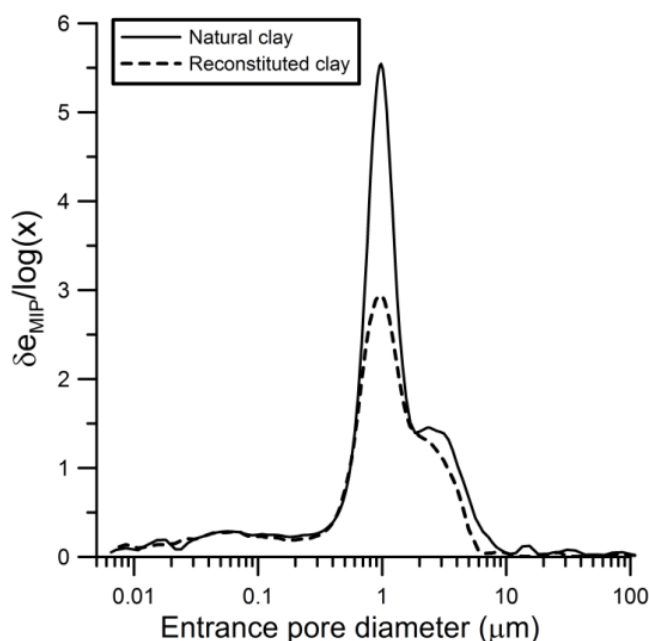
that dominant size. Hence, soil reconstitution creates a similar fabric although it erases a significant proportion of pores with the dominant size.
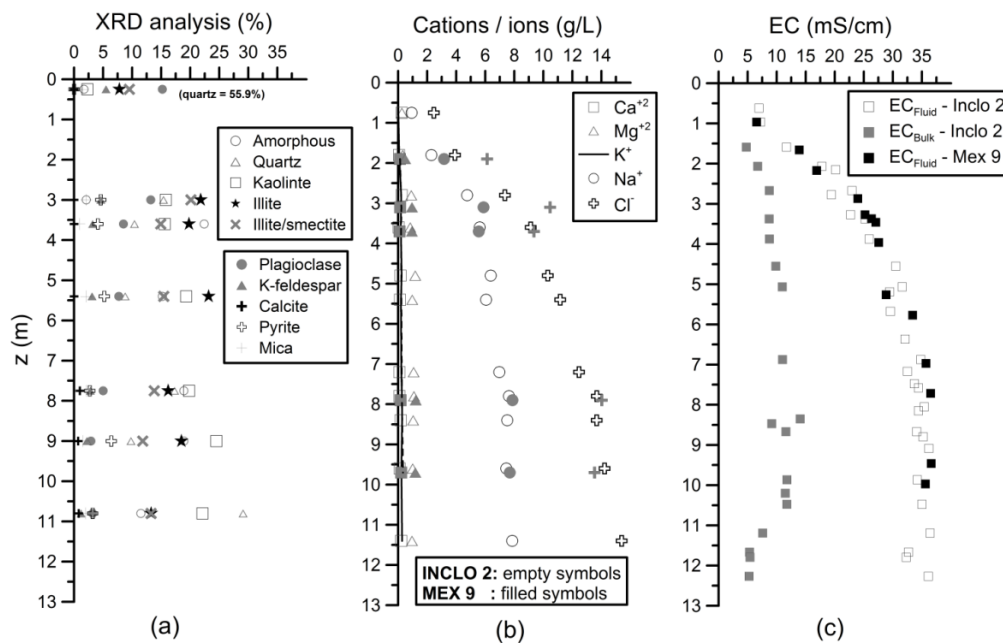
Figure 2. (a) Mineralogical composition. (b) Cations and ions. (c) Electrical conductivity.
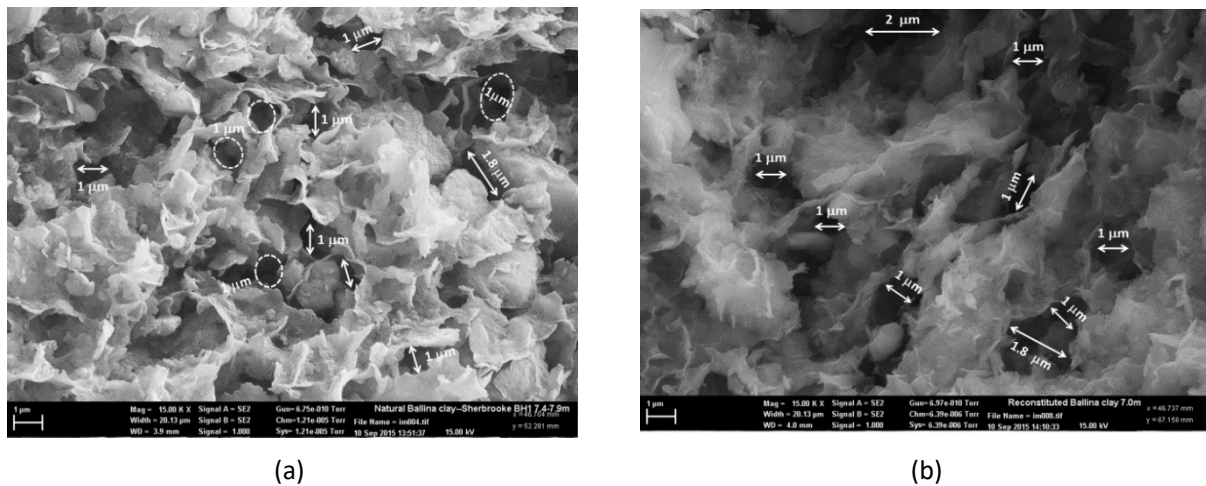
Figure 3. (a) SEM images for Sherbrooke (block) specimens of Ballina clay ($z \approx 7.5$ m). (b) SEM image for reconstituted Ballina clay ($\sigma'_{rec} = 70$ kPa).

Figure 4. MIP results for natural (Sherbrooke sample, z ≈ 7.5 m) and reconsituted Ballina clay.
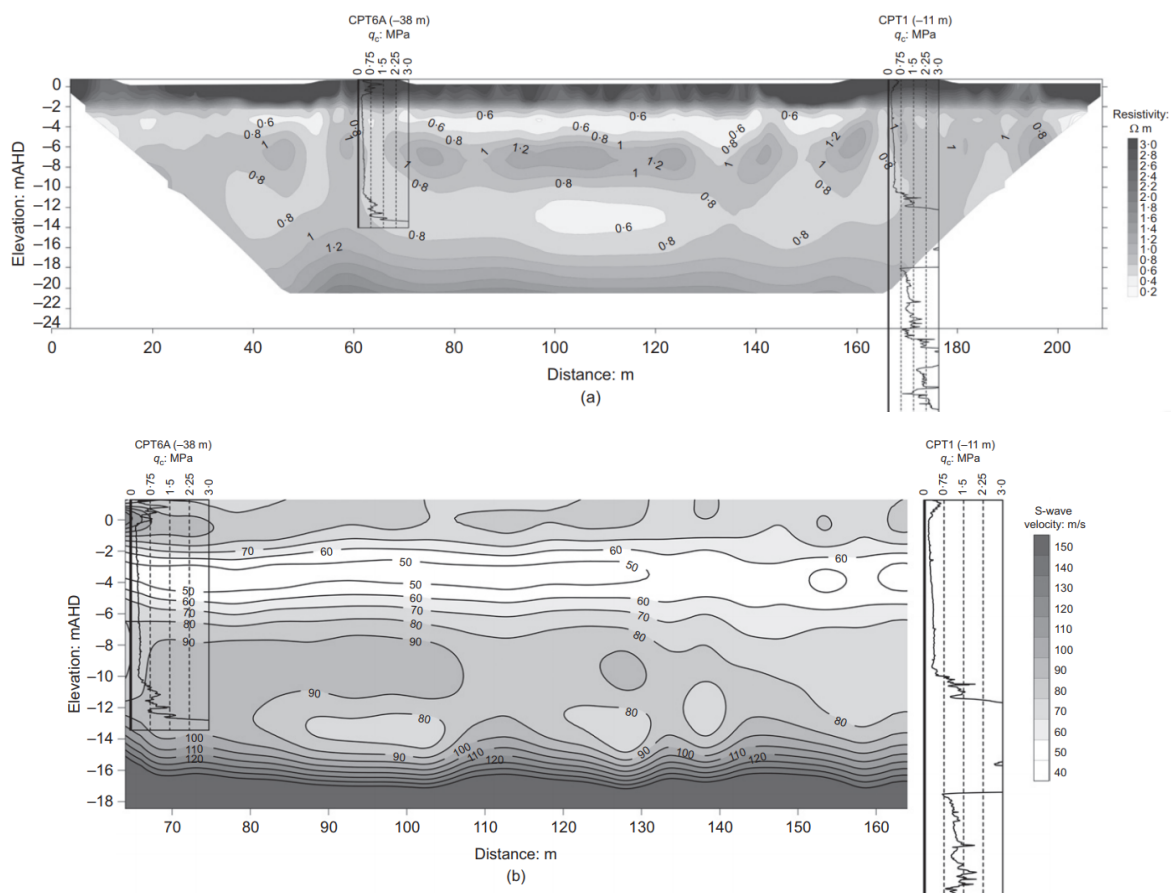
4. State and index properties

Figure 1c shows the location of the *in situ* tests performed in the characterization study. Resistivity and shear wave velocity profiles obtained from electrical resistivity imaging (ERI) geophysics and multi-channel analysis of surface wave (MASW) geophysics along north-south and east-west sections are shown in Figures 5 and 6, respectively. The results show a soil profile composed by four main layers. A shallow alluvial layer is followed by a soft clay stratum (Ballina clay). The soft clay layer is underlain by a transition zone where the sand content increases. ERI and MASW also detect a stiff clay layer below the transition zone. Although these layers seems to be uniform with depth along north-south direction, the thickness of the soft clay layer increases towards the east. The boundaries between the alluvial and the soft clay layer as well as between the transition zone and the stiff clay may be identified from ERI results. The MASW indicates the transition between the soft clay and sand at Vs between 80 m/s and 100 m/s (north-south direction) and between about 90 m/s and 100 m/s (east-west direction). As could be expected for soils deposited under a marine environment, resistivity values are low (conductivity is high).

The stratigraphic boundaries are clearly identified from the CPT data included in Figures 5 and 6. In a statistical study using CPT data, Li et al. [9] concluded that the material properties of the Ballina clay are quite uniform with distance in the horizontal direction.

Profiles of index and state properties, obtained using specimens from boreholes Inclo 2 and Mex 9, are plotted in Figure 7. Figure 7a shows an increase in the natural water content from 20% (z ≈ 1 m) up to 120% (z > 7 m). Values of liquid limit are slightly higher (10–15%) than the natural water content whereas the plastic limit ranges between 20% and 53%. Natural dry density reduces from 1.50 Mg/m^3 to 0.70 Mg/m^3 at 4.5 m depth (Figure 7b). Minor changes in ρ_d are observed between 3 m and 11 m. Differences in ρ_d between borehole Inclo 2 and Mex 9 are consistent with the difference in moisture content as a consequence of seasonal variations in the water table level as well as additional consolidation due to the thicker soil profile at borehole Mex 9.

Figure 7c shows the variation of sand, silt and clay contents with depth. At shallow depths ($z <$ 2 m), important differences in sand content are observed between boreholes. Below that level, the clay fraction is predominant with maximum values up to 82%. The change in soil stratigraphy detected from geophysics and CPT testing is confirmed here by the strong increase in sand content encountered below 11.1 m depth. As observed in Figure 7d, the density of solid particles, ρ_{solids}, lies between 2.64 and 2.68 Mg/m^3. Another feature of the soil deposits at Ballina site is the presence of organic matter, OC, which lies between 0.8 and 4% (OC$_{average} \approx 3.0$ %).

Vibrating wire piezometers (VWP) installed below the footprint of the PVD embankment indicate that the groundwater at Ballina site is hydrostatic. Total vertical stresses were calculated using bulk unit weights and specific weight of solids measurements previously shown in Figure 7. Effective vertical stresses were calculated using the total stresses and the hydrostatic pressure. Values computed for the south end of the PVD embankment are shown in Figure 8a. Push-in pressure cells (PIPC), installed at 4.35 m, 8.4 m and 12.6 m, were used to assess the coefficient of lateral earth pressure (K_0). Profiles of K_0 were estimated from SDMT and CPTu data. Further details are given in [2]. The comparison of the different K_0 estimations presented in Figure 8b shows that K_0 reduces with depth from 3 to about 0.5. A low K_0 was measured by PIPCs for the sandy layer encountered below 12 m depth. Although a clear explanation for this low value is not available it may be due to arching effects on the pressure cells.

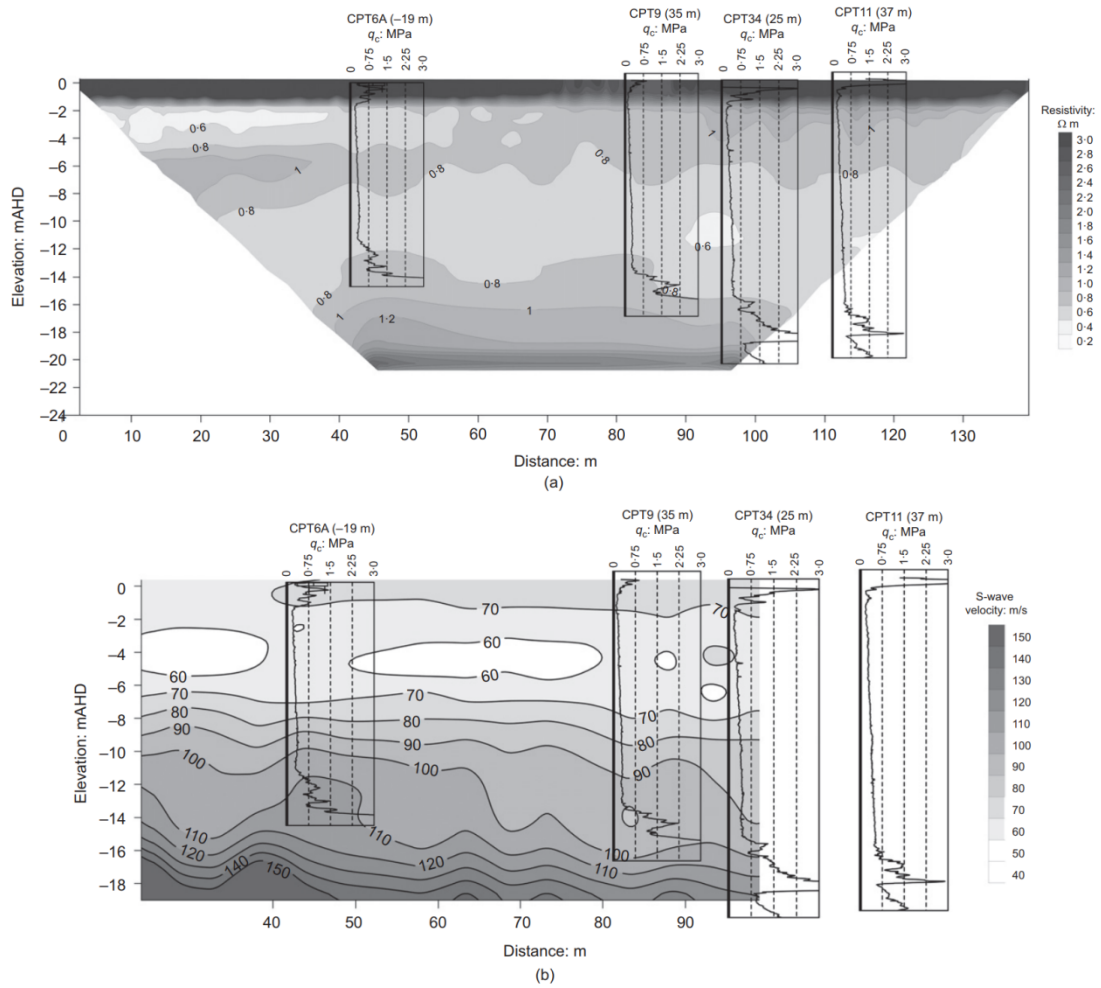**Figure 5.** ERI and MASW geophysics along north-south direction.

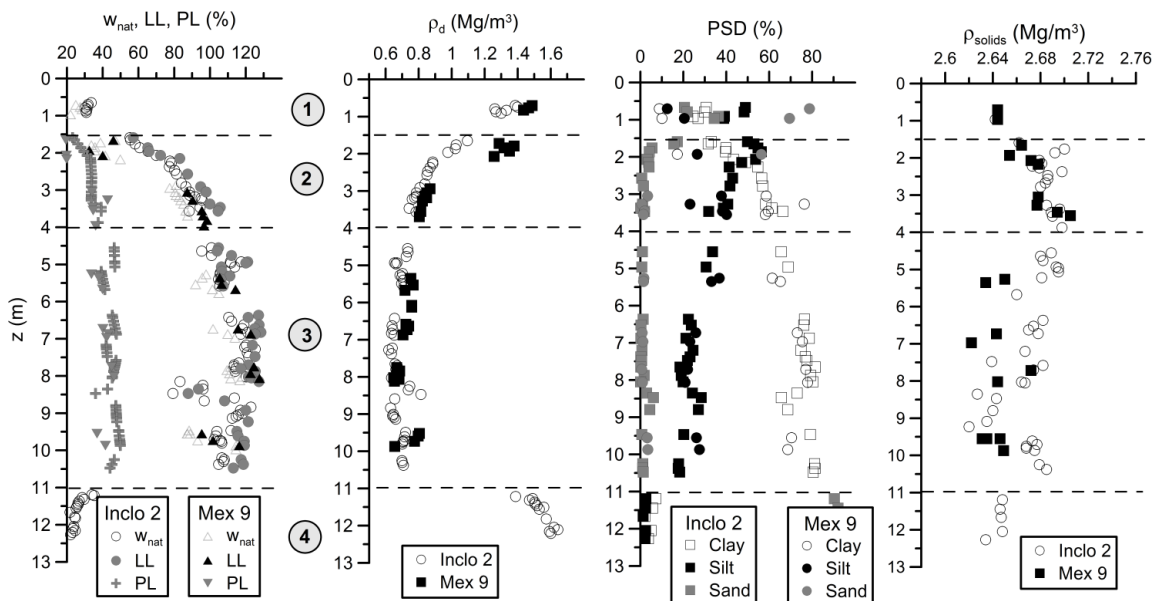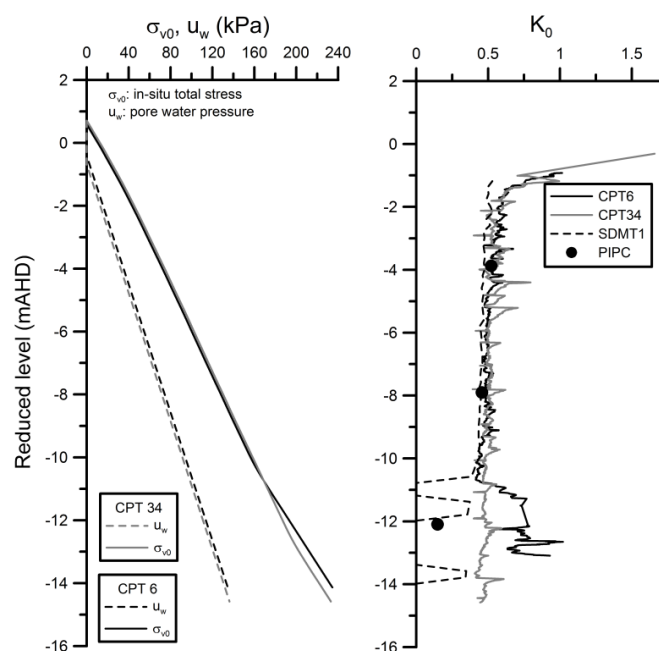**Figure 6.** ERI and MASW geophysics along east-west direction.

**Figure 7.** Variation of index properties at Ballina site.

Figure 8. (a) Variation of hydrostatic pore pressure, total and effective stresses. (b) Variation of K_0 with depth.

5. Engineering properties

The characterization study carried out at the University of Newcastle Australia for the soil deposits encountered at Ballina site [1,2], included comprehensive *in situ* testing and advanced laboratory programs aimed at obtaining the variation of engineering parameters with depth. Engineering properties were evaluated from mechanical tests carried out using tube specimens as well as high-quality block specimens [1,3]. Laboratory tests included one-dimensional constant rate of strain (CRS) tests, one-dimensional incremental loading (IL) tests and stress-path triaxial testing. It may be noted that synthetic solutions, prepared at the same salinity as the natural soil, were used in CRS, IL and triaxial tests. Laboratory results were complemented with *in situ* tests, particularly piezocone (CPTu) testing, seismic dilatometer (SDMT) and field vane (FV) tests. *In situ* tests results confirmed the uniformity of the soft clay layer, located between reduced levels of −2 m to −10 m. This is demonstrated for instance using the CPT profiles reported in Figure 9, obtained at three different locations in the NFTF (see Figure 1c).
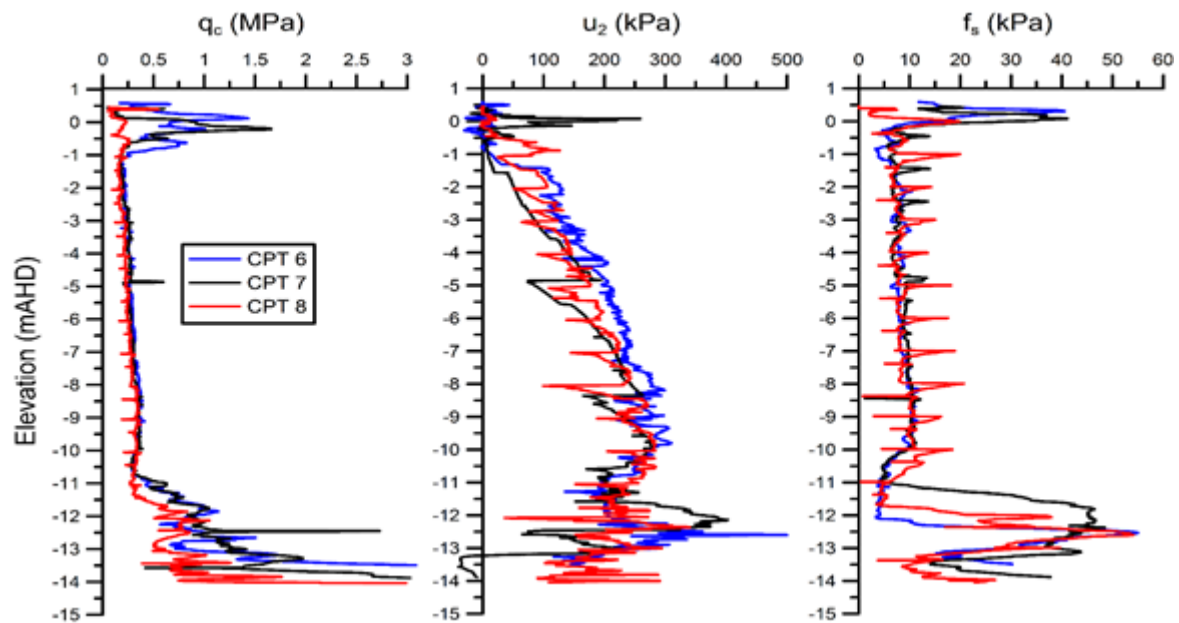
Figure 9. Profiles of cone resistance, sleeve friction and water pressure for CPT 6, CPT7 and CPT8.

Figure 10a shows compressibility curves defined in terms of the void index ($I_v = (e - e^*_{100})/C_c^*$) vs. vertical effective stress (σ'_v) for specimens used in CRS tests. The estimation of the void index requires the parameters e^*_{100} (void ratio for reconstutited soil at $\sigma'_v = 100$ kPa) and C_c^* (compression index for reconstituted soil) to be determined. Values of e^*_{100} and C_c^* for the entire profile were estimated using the empirical correlations proposed by Burland [10]. Unloading paths are not included in this figure for clarity. Solid lines and dashed lines represent specimens from borehole Inclo 2 and Mex 9, respectively. The Intrinsic Compression Line (ICL) and the Sedimentary Compression Line (SCL), proposed by Burland [10], are included as reference. Figure 10(a) includes the compressibility curves for reconstituted Ballina clay. The position of the compressibility curves above the ICL confirms the structured nature of these soft soil deposits. The sensitivity inferred from this plot ranges between 1.5 and 8. It may be noted that estimations of soil sensitivity based on liquidity index (LI = (water content − plastic limit)/plasticity index)) [11] provide values between 2 to 12. Soil destructuration is observed as the stress level increases beyond σ'_{yield} which was estimated using the strain energy method [12]. Two destructuration rates are observed in Figure 10a. Larger destructuration is observed in specimens located below 5 m (black solid lines) which is indicative of a different soil structure (fabric). This is consistent with the small variations in index and state properties observed in Figures 2 and 7 for specimens located below 5 m depth.

Figure 10b shows the strong variation in C_c estimated from the CRS test as $C_c = -\partial e/\partial \log(\sigma'_v)$ for specimens retrieved from 6.5–6.8 m depth. Discrete values ($C_c = -\Delta e/\Delta \log(\sigma'_v)$) are included in this figure for comparison. A peak value of C_c (up to 3.4) is observed at around 1.2–1.5 times σ'_{yield}. It then reduces with the stress level towards values measured on reconstituted specimens (0.9–1.2). Figure 10c shows the evolution of the consolidation coefficient, c_v, estimated from CRS test data, with the vertical effective stress. Within this range, c_v decreases with depth but also with the stress level, mainly for $\sigma'_v < \sigma'_{yield}$ due to progressive soil destructuration. c_v reduces more than one order of magnitude, from around 15 m²/year to values ranging between 0.3 to 0.85 m²/year. The estimated

water permeability (not shown here) varies with depth between 10^{-8}–10^{-11} m/s. Specimens retrieved below 4 m depth have a permeability change index between $0.8 < C_k < 1.2$ whereas at shallow depths C_k ranges around 0.2–0.5. As observed in Figure 10d, the secondary compression index $C_\alpha = \Delta e / \Delta \log(t)$, estimated from IL tests, varies from around 0.02 ($\sigma'_v < \sigma'_{yield}$) up to 0.04–0.08 for stresses around σ'_{yield}. C_α reduces to 0.025–0.040, once the yield stress has been exceeded. In general, the ratio C_α/C_c varies in a narrow band between 0.025–0.05, in agreement with the range reported by Mesri & Godlewski [13].
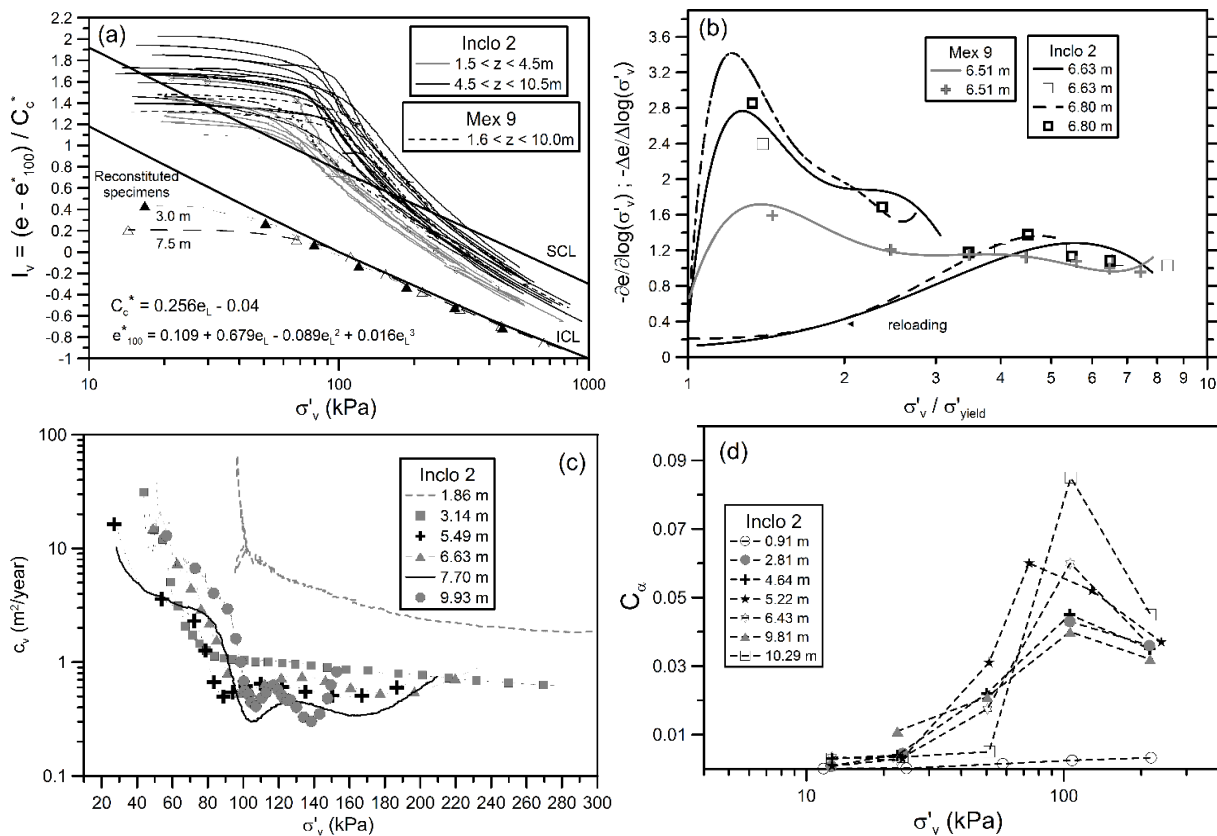
Figure 10. CRS and IL tests results on Ballina clay. (a) Compressibility curves. (b) Compression index. (c) Coefficient of consolidation. (d) Secondary compression index.

Figure 11 presents the stress paths followed in the q-p' plane for specimens subjected to undrained anisotropically consolidated triaxial (compression and extension) tests. Tests reported in this figure were performed on tube specimens retrieved with the 89 mm fixed-piston sampler as mentioned above. A brittle behaviour is displayed by the tested specimens. Triaxial compression tests provided values of peak friction angle ranging between 32° and 50° with a post-peak response characterized by secant friction angles, ϕ'_{sec}, of 32°, 36° and 41°. Friction angles around 42°–53° represent peak conditions in extension tests. On the other hand, drained shear strength parameters obtained from direct shear tests indicate that shear strength parameters equal to $\phi'_{peak} \approx 34°$ and c′ = 15 kPa and $\phi'_{peak} \approx 38°$ and c′= 0 kPa are representative of the alluvial crust (z < 1.5 m) and the sandy soils encountered between 11.1 and 12.3 m depth, respectively.
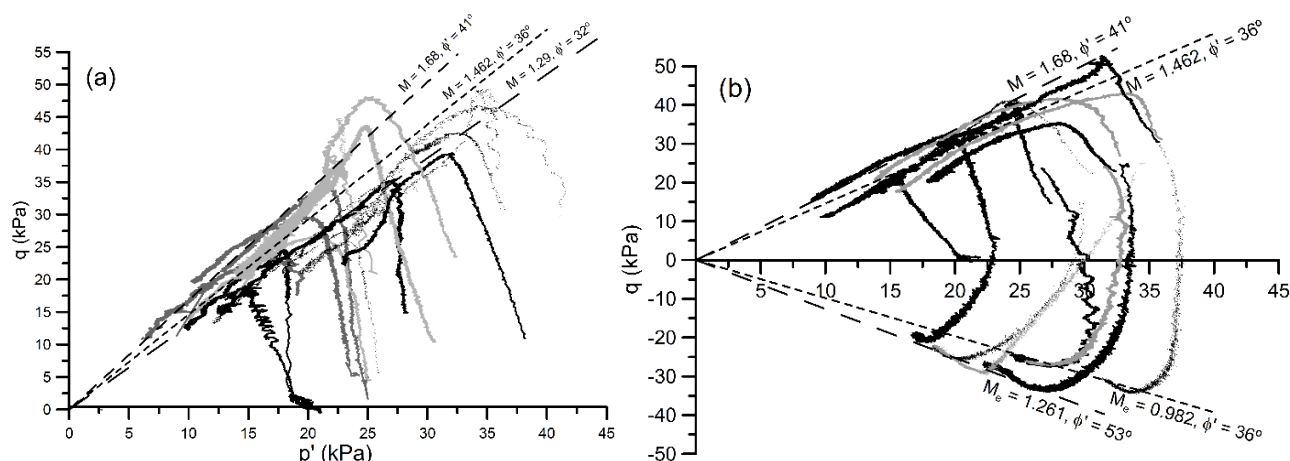
Figure 11. CK_0U triaxial tests results. (a) Borehole Inclo 2. (b) Borehole Mex 9.

Compressibility parameters estimated from CRS tests are plotted in Figure 12. Values of shear wave velocity measured at the *in situ* stress in CRS tests are also included in this figure. Values of yield stress have been corrected by rate effects according to Watabe et al. [14]. The applied correction factor was 0.84. The yield stress ratio, $YSR=\sigma'_{yield\text{-}corrected}/\sigma'_{v0}$, decreases with depth from 2.5 to 1.4–1.5. YSR is larger for borehole Mex 9, in agreement with differences in water content as discussed above.

Figure 12c compares laboratory shear wave velocity measurements with *in situ* values estimated from SDMT tests (SDMT-1 and SDMT-34). Laboratory measurements of the shear wave velocity reported in this figure were obtained at the *in situ* vertical stress during CRS tests via bender elements transducers. The time domain analysis [15,16] was adopted for the estimation of the arrival time of the shear wave. The good agreement between *in situ* and laboratory data is indicative of the good quality of the tested specimens. Laboratory measurements picked up the increase in Vs detected in SDMT-1 (at the end of the PVD embankment) below 11 m depth, where a sand layer is encountered.

Estimations of horizontal and vertical coefficients of consolidation were obtained from *in situ* (CPTu) as well as laboratory (CRS) tests. In the former case, c_h was evaluated using the curve fitting technique described in Teh & Houlsby [17]. Values of c_v estimated at yield stress are reported in Figure 12 in in addition to c_h estimates. Similar values are observed between c_h and c_v both ranging between 1.5 m^2/yr and 15 m^2/yr. Minor differences between c_h and c_v (k_h and k_v) indicate a low permeability anisotropy for Ballina clay. This aspect has been previously recognized for homogeneous marine clays [18].
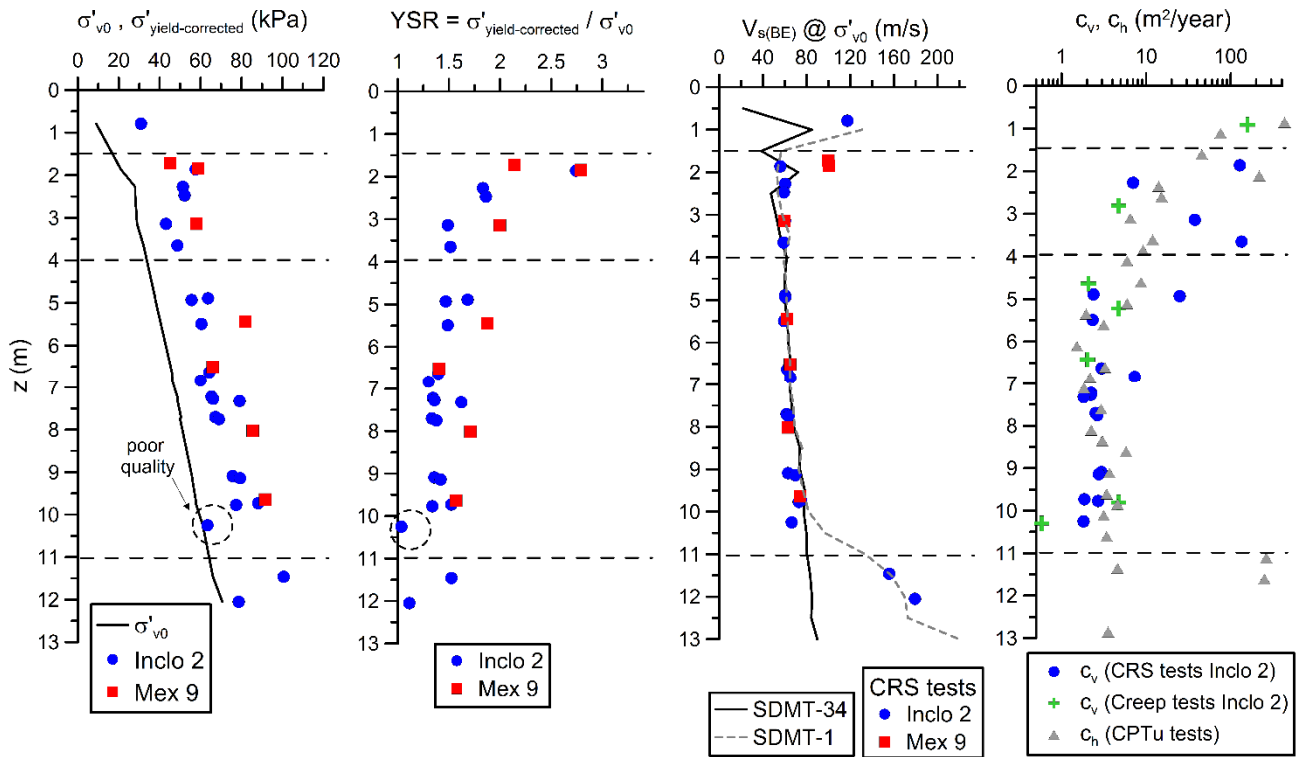
Figure 12. Geotechnical profiles: compressibility parameters and shear wave velocity at *in situ* stress state.

Figure 13 compares values of peak undrained strength, s_u, derived from laboratory (see Figure 11) and *in situ* tests. Shear strength interpreted from cone penetrometer (CPTu), seismic dilatometer (SDMT) and field vane shear (FVS) tests are included in Figure 13b. The N_{kt} factor used to convert the CPTu data to FV strength was 13.2. Undrained shear strength data shows that s_u is greatest in triaxial compression, intermediate in vane shear and least in triaxial extension. The variations with depth are 8.4 kPa + 2z for depths between 1.5 m and 8 m (triaxial compression) and 10.7 kPa + 1.2z between 3.5–10 m (triaxial extension) (Figure 13a, where z is the depth in metres). Between 4 < z < 11 m, the ratios $s_{u\text{-}TC}/\sigma'_{yield}$ and $s_{u\text{-}TE}/\sigma'_{yield}$ are equal to 0.325 and 0.235, respectively. These values are consistent with those reported in the literature for inorganic soils [19,20]. The ratio between $s_{u\text{-}TE}/s_{u\text{-}TC,}$ estimated using specimens from borehole Mex 9 (3 < z < 10 m), gives an average ratio around 0.66. This value falls within the range of variation reported by Won [21] for marine soft clays. Peak vane shear strength varies linearly increasing with depth according to: 12.5 kPa + 0.8z (z > 1.5 m). The sensitivity of the soft soil deposits, estimated from peak and residual vane strengths ranges around 2–4, lower than the range of variation obtained from one-dimensional compression tests (1–8).
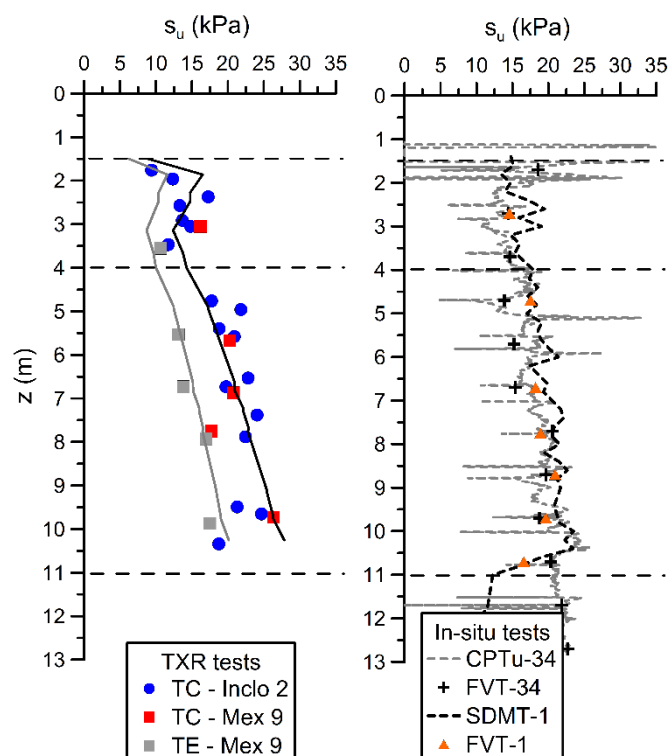
Figure 13. Undrained shear strenght profiles. (a) Laboratory triaxial tests. (b) *In situ* tests (CPTu, SDMT and FVT).

6. Sampling disturbance assessment

The evaluation of soil disturbance caused by sampling is a complex phenomenon due to the contribution of the different stages involved in a sampling campaign. Therefore, the combination of different techniques, non-destructive measurements and mechanical tests, seems adequate to get complementary information that may help to improve the quality of the mechanical properties estimated from laboratory tests. The following approaches have been employed to evaluate the quality of Ballina clay specimens (block and tubes):

✓ Mechanical tests: variation in void ratio after recompression to *in situ* stress $\Delta e/e_0$ [22]
✓ Shear wave velocity measurements
✓ Image analysis (CAT imaging)
✓ Microstructural analysis: mercury intrusion porosimetry (MIP)

Figure 14a shows the values of the ratio $\Delta e/e_0$ for 55 specimens, obtained with a fixed piston sampler (89 mm in diameter), tested under CRS and triaxial conditions. Most of the specimens (47) are of very good to excellent quality, 8 specimens are of good to fair quality, and only 3 are of poor quality. Figure 14b shows values of shear wave velocity at the *in situ* vertical stress normalized by the *in situ* value (calculated from SDMT tests) versus $\Delta e/e_0$. The sample quality index $\Delta e/e_0$ increases with decreasing the normalized shear wave velocity. Specimens rated as good to excellent quality display a normalized velocity ranging from 0.85 to 1.02 (0.96 on average). Poor quality specimens have a normalized velocity around 0.75. Results shown in Figure 14 confirm the reliability of the fixed-piston sampler in providing good quality specimens.
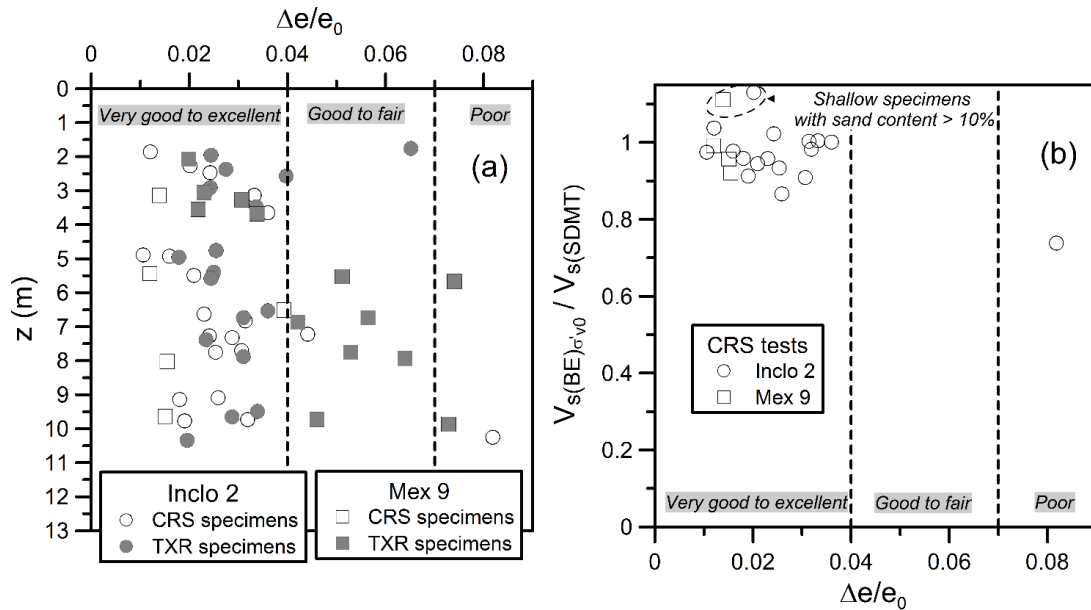
Figure 14. Sample quality assessment (89 mm fixed-piston samples). (b) Normalized void ratio. (b) Normalized shear wave velocity vs normalized void ratio.

Computer Axial Tomography (CAT) imaging is becoming an interesting tool to inspect, in a non-destructive way, the condition of tube specimens prior to laboratory testing. An example of the use of CAT scans on Ballina clay specimens is given in Figure 15. This figure compares vertical sections for four tube specimens obtained using Shelby tubes (U75), a free-piston sampler (P100) and an Osterberg fixed-piston sampler (O89). Specimens were obtained between 7.5 m and 8.1 m depth. Table 1 summarizes the main characteristics of tube samplers. There, B refers to the external sampler diameter, t is the thickness of the tube wall, α is the angle of the cutting shoe, AR is the area ratio (area of the annulus of the tube sampler divided by the area of the tube specimen) whereas ICR is the inside clearance ratio (the enhancement of the internal tube diameter behind the cutting edge). Table 1 also includes the characteristics of a 50 mm Shelby tube employed in a microstructural study described below. CAT scans were obtained using a commercial medical CAT scanner. The attenuation scale varies from white (high material density) to black (low density). Figure 15 shows that Shelby tubes (U75) produce highly disturbed specimens with sub-horizontal cracks, fissures and cavities. A well-defined pattern of sub-horizontal cracks is observed along the entire specimen for the sample retrieved with the free-piston sampler (P100). On the other hand, 'homogeneous' (i.e. less disturbed) samples are retrieved with the fixed-piston sampler (O89). Only a few sub-horizontal cracks, located at top and bottom ends, may be observed. These qualitative results remark the need for using fixed-piston samplers in soft clays.

Table 1. Characteristics of tube samplers employed at Ballina site.

Sampler type	B (mm)	α (°)	AR (%)	B/t	ICR (%)
50 mm Shelby (U75)	51.2	12	14	31	0
75 mm Shelby (U75)	76.7	15	9	49	0
89 mm fixed-piston (O89)	89.4	13	10	45	0
100 mm free-piston (P100)	100	90	13.2	33.3	0

Shelby (U75)   Shelby (U75)   Free-piston (P100)   Fixed-piston (O89)
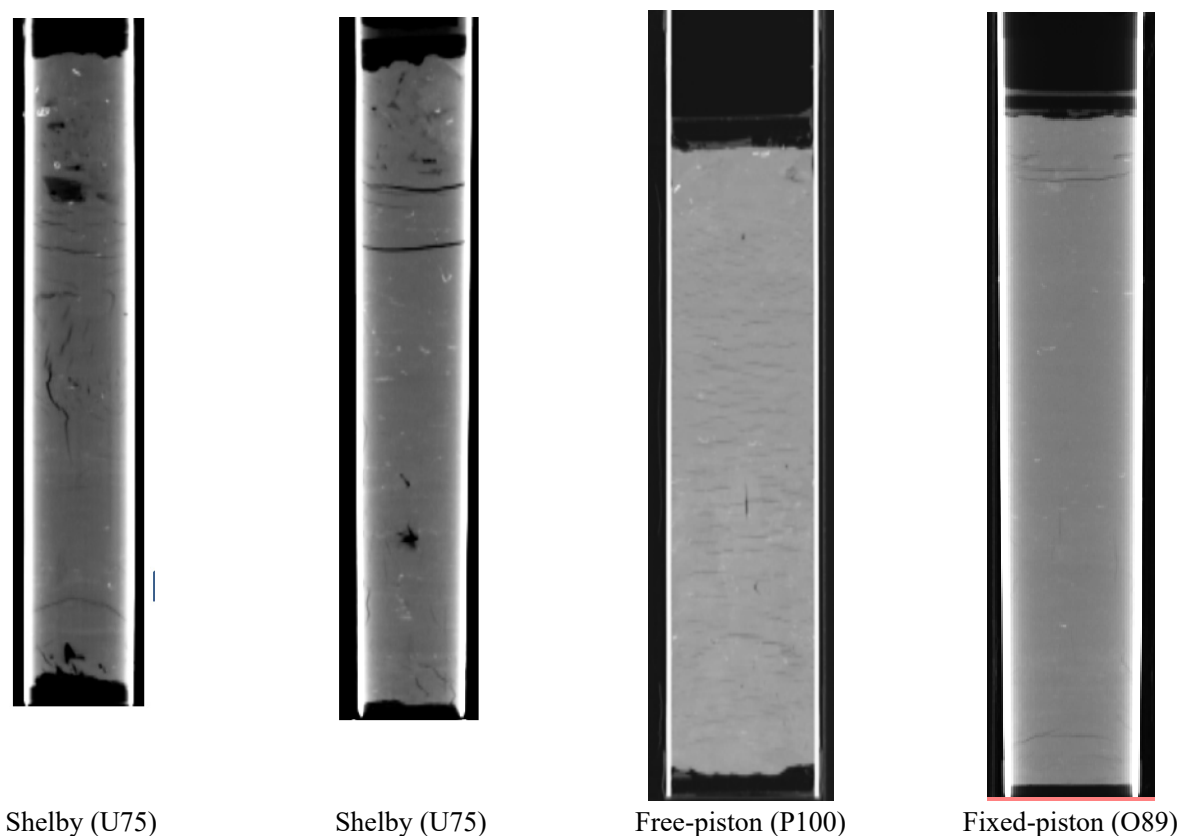
Figure 15. CAT scans of four tube specimens (z ≈ 7.5–8.1 m).

An important effect of the sampling process is the phenomenon of water content redistribution caused by the dissipation of the excess pore pressure generated by the penetration of the tube sampler into the ground. Therefore, changes in soil microstructure (fabric) are related to the combined effects of tube penetration and moisture redistribution. Pineda et al. [3] studied the influence of tube sampling on the microstructure of Ballina clay. They estimated the spatial variation in water content and void ratio for tube specimens retrieved with Shelby tubes (U50 and U75) and a fixed-piston sampler (O89). These results were complemented with mercury intrusion porosimetry (MIP) tests [23] carried out on small sub-samples (5 × 5 × 5 mm) trimmed at five levels along the centerline and the perimeter of each tube. Void ratio and water content measurements carried out on tube specimens (Figure 16a) demonstrate that Shelby samples display a non-homogeneous void ratio and water content distribution. Void ratio reduces from the top to the bottom of the tube. On the other hand, the variation of void ratio and water content in the O89 fixed-piston sample seems symmetric between upper and bottom halves. Taking into account that fully saturated conditions prevail, Figure 16a suggests that water content redistribution has occurred after sampling. Higher void ratios are observed at the centerline. This is due to the dissipation of the positive excess pore pressure and the water content redistribution [24]. This phenomenon is less pronounced in the O89 tube, indicating the beneficial effect of using fixed-piston sampler for reducing soil disturbance.

Figure 16b compares the pore size density (PSD) curves estimated from MIP tests for specimens retrieved at levels A (bottom end), C (middle) and E (top end) from the centerline and the

perimeter of each sampler. It may be noted that the PSD of the Sherbrooke specimen is also included in Figure 16b as reference. New macro pores and modifications to the PSD, with respect to the one for the Sherbrooke sample, are observed at levels E and A. This effect is more evident in Shelby tubes. Similar PSD curves are observed for specimens located at level C. This demonstrates that less disturbance occur for the soil close to the centreline of the tube. The PSDs shown in Figure 16b reflect three main deformation mechanisms as follows: (i) the reduction of the peak density suggest a decreasing in the number of pores with the dominant size (e.g., by compression), (ii) an enhancement of the macro porosity due to the increase in the dominant pore size, and (iii) the creation of new macro porosity, identified by the appearance of secondary peaks in the PSD at large entrance pore sizes. At level C on the centreline, only mechanisms 1 and 2 are significant. This implies that axial deformation is the factor that controls sampling disturbance. The creation of new peaks at the top and bottom ends on the centreline point out a complex deformation pattern (involving mechanisms 1, 2 and 3) that also occurs in specimens located at the perimeter of the sampler. The important variations in the dominant pore diameter for each tube sampler are plotted in Figure 17. The fact that the O89 fixed-piston sampler shows the smallest variation in the dominant pore diameter confirms the beneficial effect of using large-size tube samplers and the strong influence of the piston in reducing soil disturbance.
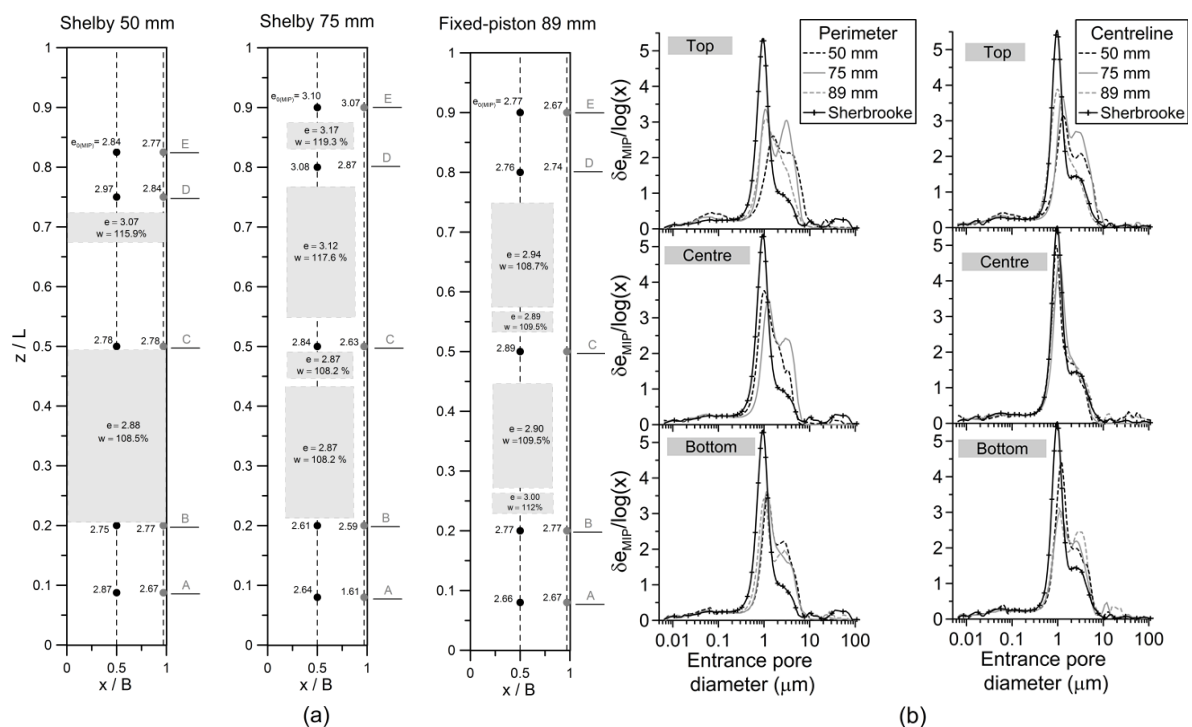
Figure 16. Microstructural changes due to tube sampling in Ballina clay. (a) Variation in moisture content and void ratio. (b) PSD curves for levels A, C and E (centreline and perimeter).
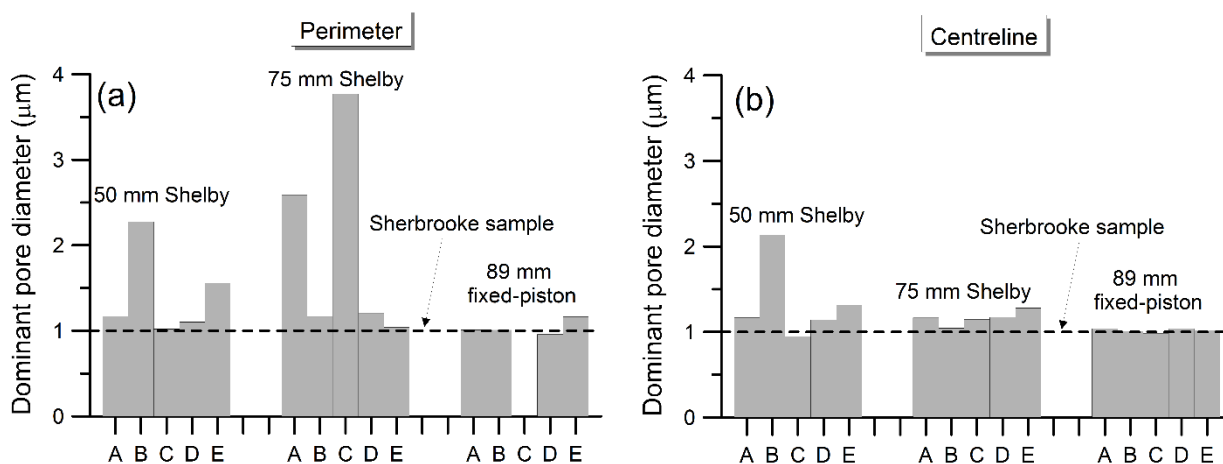
Figure 17. Variation of the dominant pore size. (a) Perimeter. (b) Centreline.

In a recent study, Lim et al [25] evaluated the influence of sampling disturbance on the mechanical properties of Ballina clay estimated from laboratory tests. They tested tube specimens retrieved with   a Shelby tube (U75), a free piston sampler (P100) and a fixed-piston sampler (O89) retrieved at the NFTF from a depth of 5.5 to 6.1 m. CRS tests as well as simple shear (SS) tests with cell pressure control were performed. The behaviour of tube specimens was compared against tests results obtained on high-quality Sherbrooke specimens. Figure 18a presents the evolution of the volumetric strain with the vertical effective stress obtained from CRS tests. Block and O89 specimens show the lowest volumetric deformation at $\sigma'_{\text{v-in situ}}$ (less than 1.7%) followed by the P100 and U75 specimens, respectively. This behaviour is also evident in terms of the larger yield stress σ'_{yield} (indicated as grey stars) (Figure 18b). It may be noted that the yield stress obtained from the U75 specimen (~20 kPa, i.e. OCR < 1) is incompatible with the stress history of the deposits at the NFTF. Specimen P100 shows a σ'_{yield} slightly higher than $\sigma'_{\text{v-in situ}}$, thus, much lower than the OCR reported by Pineda et al. [1] (see Figure 11).

The oedometric modulus, M, as well as the compression index, C_c, are strongly reduced by sampling disturbance. Figure 18c shows that the oedometric modulus reduces from 2.72 MPa (block sample) to 0.25 MPa (U75 sample). Block and the O89 specimens follow a similar trend. Figure 18d demonstrates that sampling disturbance reduces dramatically the peak in C_c, achieved between 1.20–2.0 σ'_{yield}, whereas the post peak value is similar for all specimens. Block and the O89 samples provide the highest C_c followed by the P100 and the U75 specimens with values about 2 times lower than the C_c of the block sample.

The results of simple shear tests are shown in Figure 19. Block and O89 specimens show the lowest volumetric strain upon K_0 recompression to the *in situ* stress (see Figure 19a). This value is 2 and 3.3 times smaller than the deformation measured in P100 and U75 specimens, respectively. The stress-strain curves obtained from the undrained shearing stage (Figure 19b) show small variation in the peak shear stresses irrespective of the sample provenance. This behaviour is due to the differences in void ratio achieved at the end of the consolidation stage (larger volumetric compression for U75 and P100 specimens). The influence of sampling disturbance is clearer in terms of the peak shear strain between block and U75 specimens.

Mechanical parameters obtained from the CRS and SS tests described above are compared against the sample quality index $\Delta e/e_0$ in Figure 20. The trend shown in Figure 20 is qualitatively

consistent with published data, i.e. the estimated σ'_{yield}, initial M and $C_{c\text{-peak}}$ decrease with reducing sample quality. However, the P100 specimen classifies as good to fair quality which would imply that results from this specimen could be used with confidence in design. This result would appear to be a misleading outcome based on the behaviour of the P100 specimen with respect to block or O89 samples.

Peak undrained shear strength, $\tau_{xy\text{-peak}}$, shear strain at peak, γ_{peak}, as well as the undrained secant modulus at 50% of $\tau_{xy\text{-peak}}$ are plotted against $\Delta e/e_0$ in Figure 20. The value of shear strain measured at $\tau_{xy\text{-peak}}$ for the U75 specimen is 4 times larger than that of the block sample. The P100 specimen classifies here as good to fair quality which is in conflict with its mechanical response against block and O89 specimens.
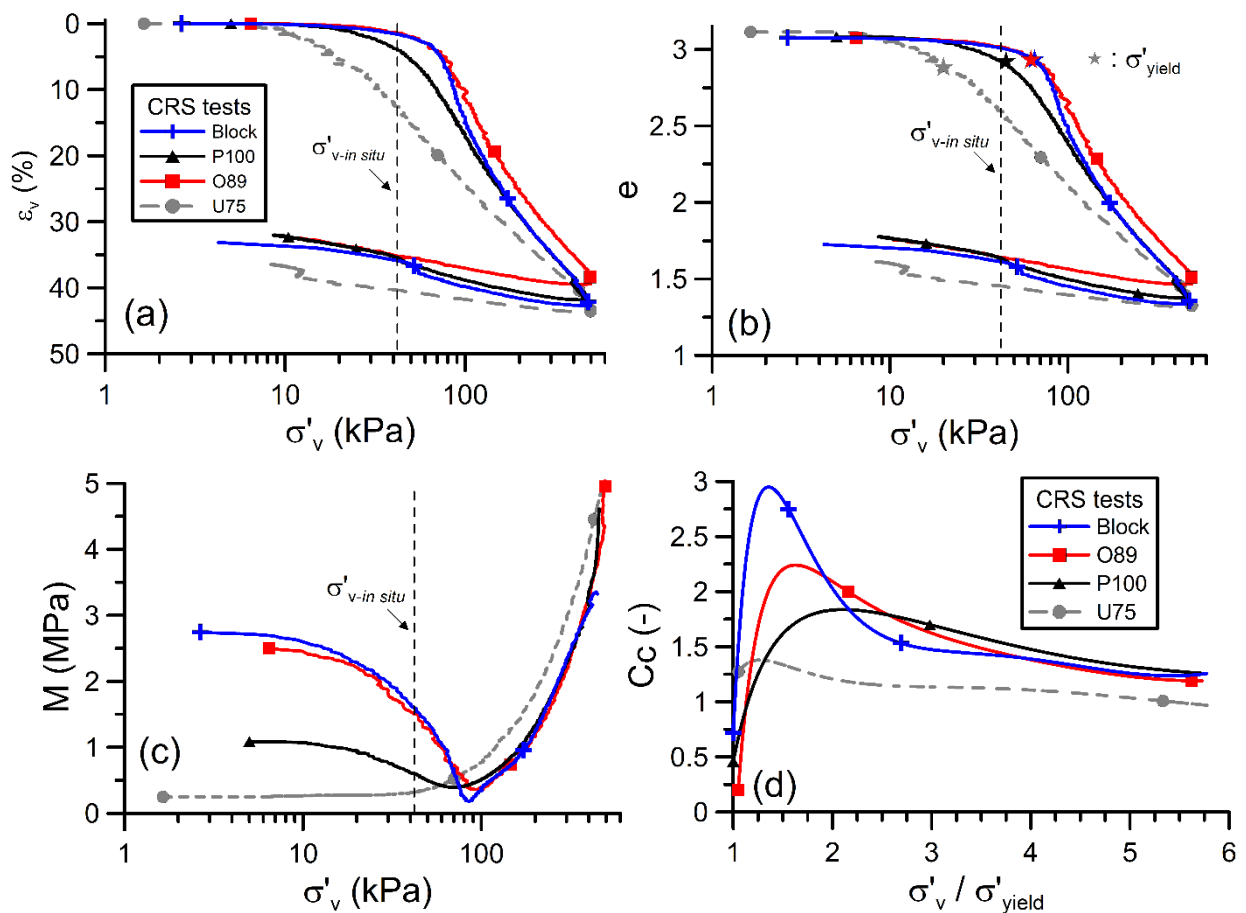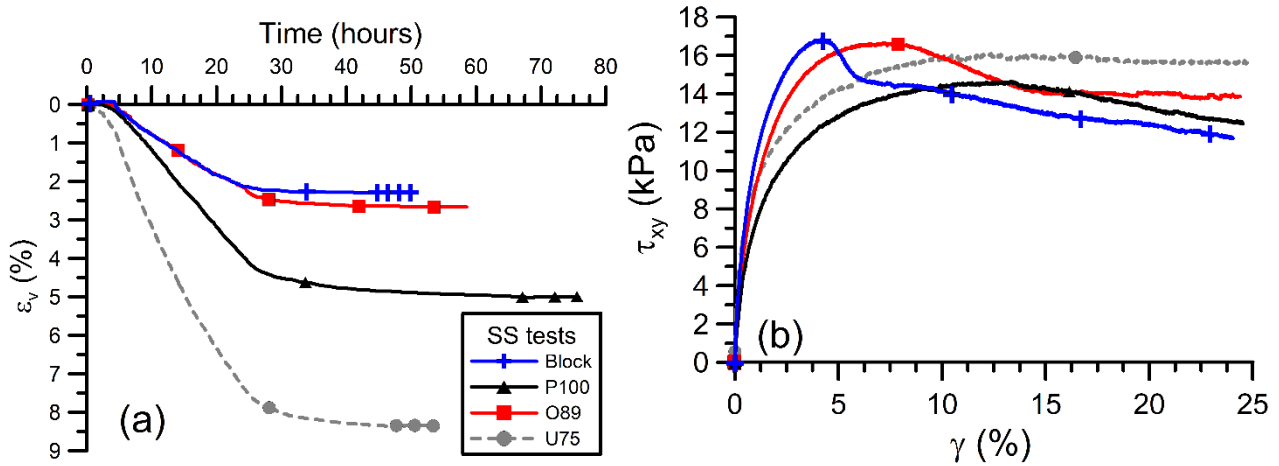

Figure 18. CRS test results.
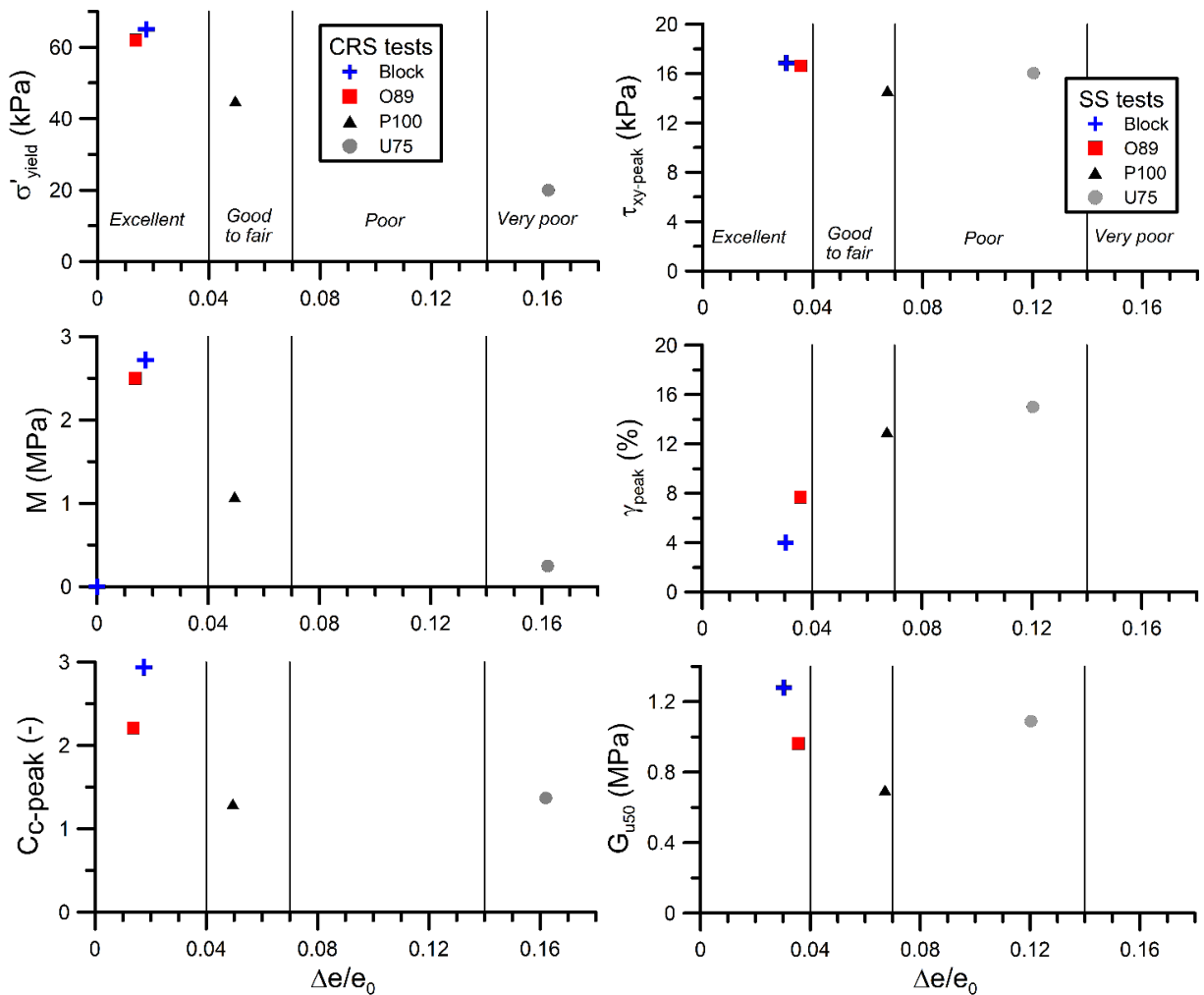
Figure 19. Simple shear tests results.

Figure 20. Comparison between mechanical properties and the normalized change in void ratio.

Lim et al. [25] carried out settlement predictions for a synthetic embankment as well as bearing capacity estimations for a shallow footing using the sets of mechanical parameters obtained for each sampler type. They found that the settlement prediction is strongly influenced by sampling disturbance due to the reduction in σ'_{yield} and C_c. This may lead to correct predictions but for the wrong reasons (which by no means reflects good practice), for instance when the reduction in C_c is largely compensated for by the reduction in σ'_{yield}. Based on the results obtained from SS tests, it was noticed that the predicted undrained bearing capacity is less affected by sampling disturbance, despite the important differences in stress-strain behaviour observed in the SS tests. Nevertheless, it may be noted that this conclusion should be confirmed for other shearing modes than simple shear due to the fact that bearing capacity is affected by strength anisotropy.

7. Newcastle symposium for the prediction of embankment behaviour on soft soil

The establishment of the NFTF by the ARC Centre of Excellence for Geotechnical Science and Engineering (CGSE) near Ballina was motivated by the difficulties encountered during the construction of a nearby motorway section. Embankments with maximum fill height 14 m settled up to 6.4m over a period of 3 years, while accurate prediction of settlement magnitude and rate of evolution of embankment deformations proved to be challenging [26]. Two full-scale trial embankments were constructed in 2013 at the NFTF, one on subsoil improved with vertical drains (PVD). This embankment was extensively instrumented both during and after construction. Measurements of pore pressures, vertical and horizontal deformations, as well as vertical and lateral soil pressures, were obtained at different locations over a period of 3 years. Accordingly, an international symposium was held in Newcastle, in September 2016, to predict the embankment behaviour. The CGSE prediction symposium received 28 'Class A' predictions from Australian and international academics and practitioners. Lessons learned from this symposium are summarized in Kelly et al. [4].

Figures 21 and 22 show, respectively, the plan view and the cross section of the PVD embankment. The embankment is 3 m in height, 80 m long by 15 m wide and battered slopes at 1.5H:1V. The embankment required the construction of a working platform (95 m long, 25 m wide and 0.6 m thick) which includes a sand drainage layer (0.4 m thick) placed beneath its footprint. Vertical drains were placed on a nominally 1.2 m square grid. Additional instruments were installed along the centerline of the embankment as indicated in Figure 22.

2D numerical analysis was the most common approach employed in the settlement prediction (57%) followed by 1D consolidation analysis (34%). Only 9% of the predictors performed 3D numerical simulations of the embankment behaviour. Figure 23a compares predicted vs measured settlements estimated from settlement plates. In general, the settlement predictions were lower than the *in situ* measurements. The total settlement ranged between 0.45 m and 1.40 m after 3 years. Two main stages may be observed in Figure 23a. The rate of settlement post-construction was overpredicted and then it was generally underpredicted for t > 1 year. The near-surface pore pressures were predicted reasonably well. However, an overestimation of the rate of pore pressure dissipation was the common trend observed at depths of 6 m (Figure 23b) and 10 m. The lateral deformations (measured and predicted) at the end of filling and after 3 years of consolidation (Figure 24) show an overprediction at the end of construction and underprediction after 3 years.

Predictors were subsequently invited to carry out a back-analysis ("Class C") aimed at explaining the reasons for the discrepancies observed in the 'blind' predictions and deriving lessons for practitioners and academics. The symposium demonstrated that, contrary to what should be expected, the selection of soil parameters for geotechnical design from *in situ* and laboratory tests involves a very high degree of subjectivity. A number of practitioners tended to resort to experience and rules of thumb when selecting the key soil parameters, which caused a large variation in the predictions. Rate effects on mechanical parameters such as the preconsolidation pressure and the undrained shear strength are concepts that seem not well rooted in practice. A systematic overestimation of the soil permeability (by around 1 order of magnitude) was observed from the predictions. A key message from the symposium is the need for a systematic process that would ideally include the use of high quality sampling techniques in combination with high quality laboratory and *in situ* testing data, the adoption of an appropriate constitutive model, and the detailed calibration of the constitutive model using element test results. Kelly et al. [4] made recommendations that, although some of these steps may sound obvious, the symposium demonstrated that not all of these steps were commonly followed.
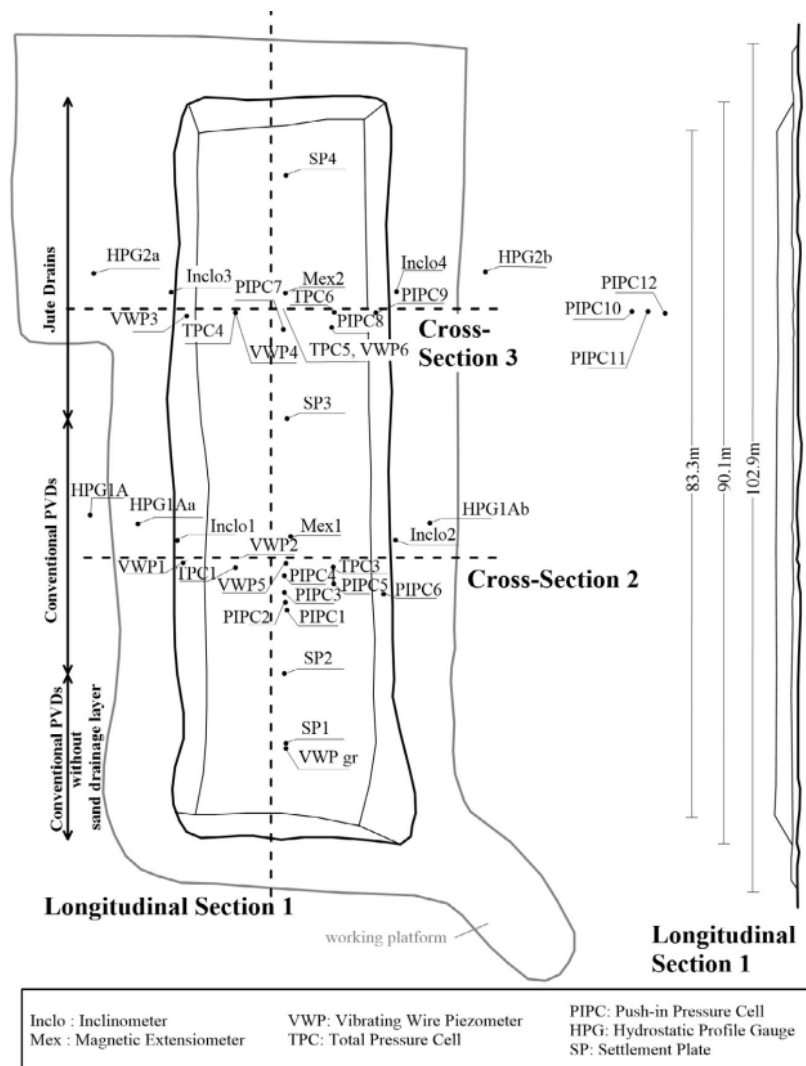
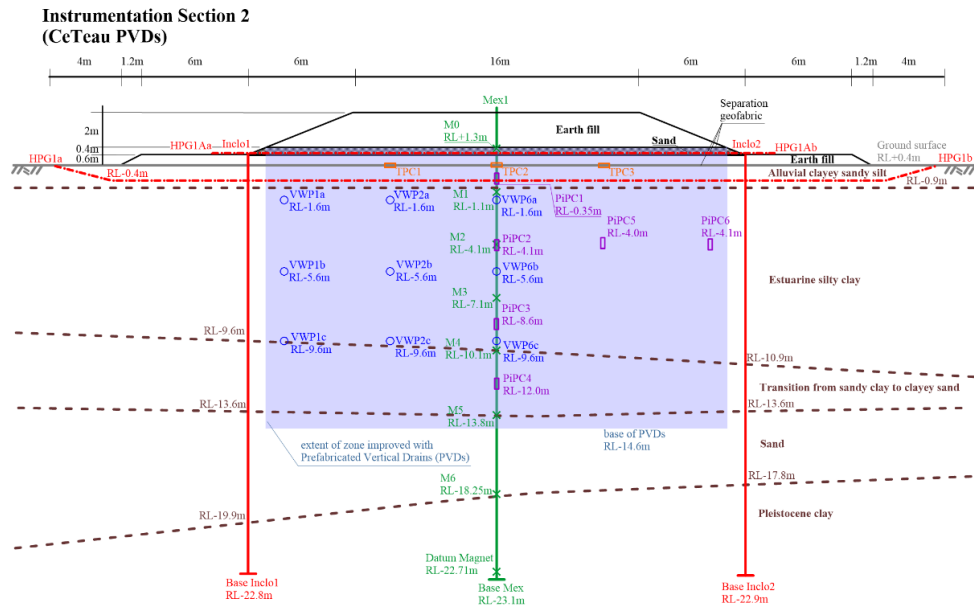**Figure 21.** Plan and elevation of the PVD embankment post construction.

Figure 22. Nominal cross Section 2, locations of instruments and soil stratygraphy.
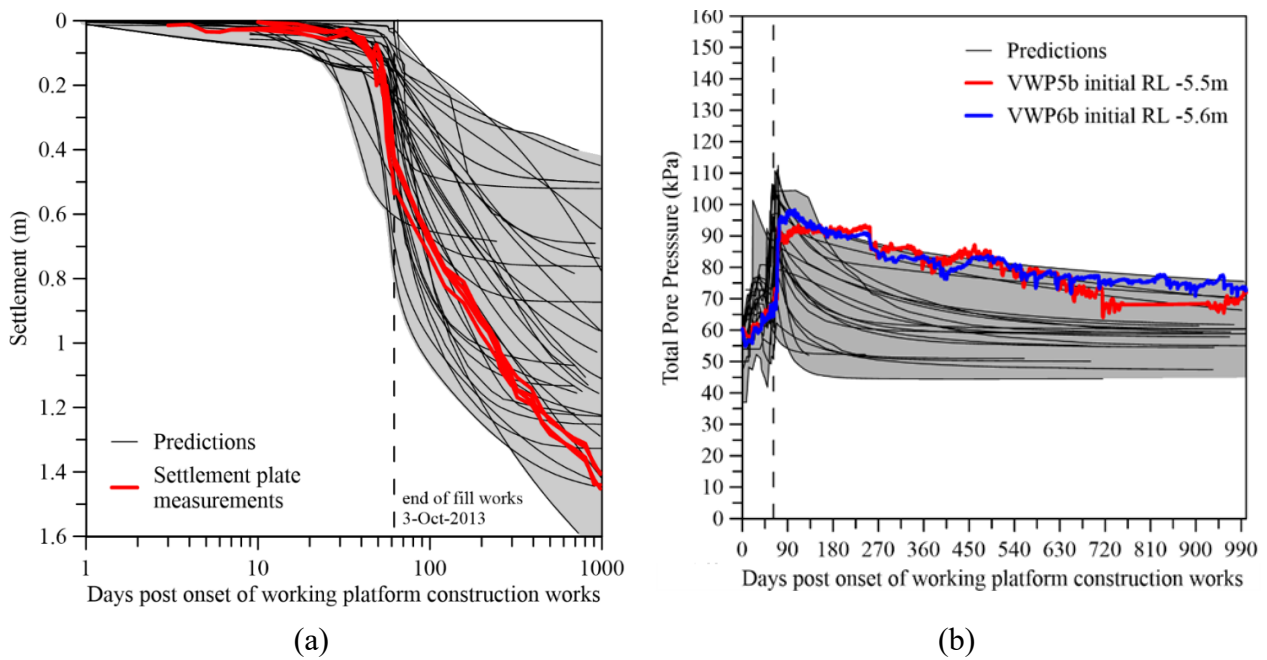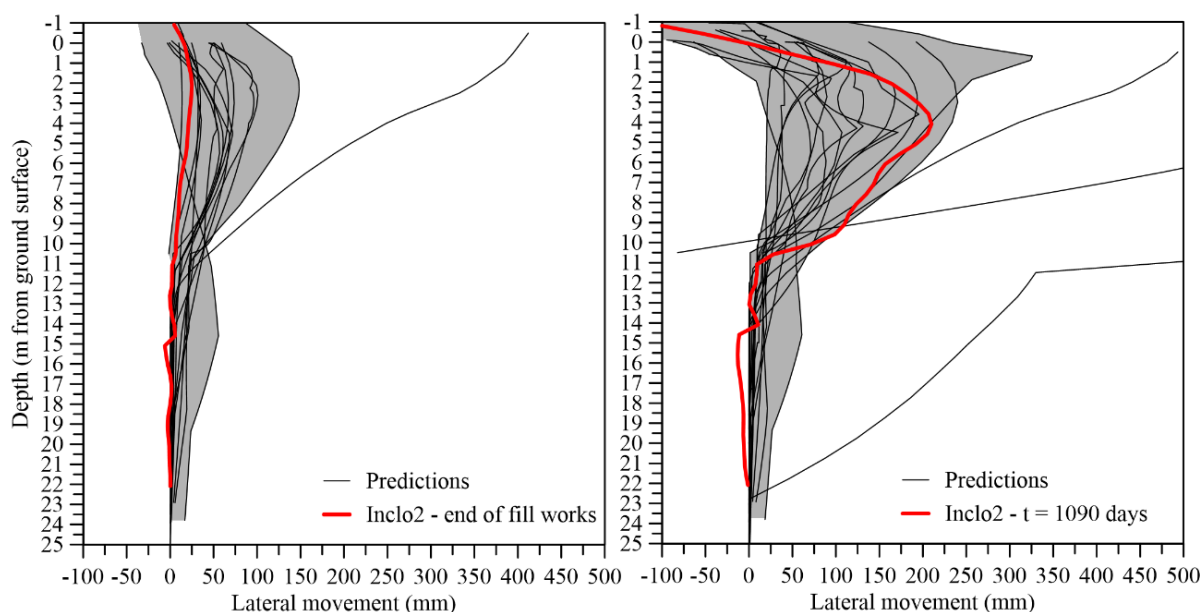

Figure 23. Measurements vs predictions of the embankment behaviour. (a) Total settlement. (b) Excess pore pressure.

Figure 24. Measurements vs predictions of the lateral deformation.

8. Concluding remarks

The establishment of the National soft soil Field Testing Facility (NFTF) at Ballina (NSW) has allowed thorough *in situ* investigations to be combined with advanced laboratory tests on high-quality samples to characterise a representative Australian estuarine soft clay. A wide range of research projects has been carried out over the past five years at the NFTF including the assessment of sampling disturbance and their consequences on the representativeness of soil parameters measured from laboratory tests which are used in geotechnical design. The NFTF has provided a unique opportunity of evaluating the current practice for predicting the behaviour of embankments and shallow footings constructed on soft soils. The prediction symposium demonstrated that further research is still necessary to improve available geotechnical design methods.

A vast amount of high-quality data obtained from *in situ* testing, sampling and laboratory testing campaigns has been produced over the last five years using the NFTF. This information has been released to practitioners and the academic community through the web page of the CGSE but also using novel online platforms for storing, managing and sharing data [27]. It is envisaged that the NFTF will continue to provide advances in design methods and site investigation technologies for years to come, ultimately leading to cheaper and more reliable transport and energy infrastructure

Acknowledgments

Conflict of interest

All authors declare no conflict of interest.

References

1. Pineda JA, Suwal L, Kelly RB, et al. (2016a) Characterization of the Ballina clay. *Geotechnique* 66: 556–577.
2. Kelly RB, Pineda JA, Bates L, et al. (2017) Site Characterisation for the Ballina Field Testing Facility. *Géotechnique* 67: 279–300.
3. Pineda JA, Liu XF, Sloan SW (2016b) Effects of tube sampling in soft clay: a microstructural insight. *Geotechnique* 66: 969–983.
4. Kelly RB, Sloan SW, Pineda JA, et al. (2018a) Outcomes of the Newcastle symposium for the prediction of embankment behaviour on soft soil. *Comput Geotech* 93: 9–41
5. Loughnan FC (1969) Chemical weathering of the silicate minerals. Elsevier, New York.
6. Bishop DT (2004) A proposed geological model and geotechnical properties of a NSW estuarine valley: a case study, In: Proc. 9th ANZ conference, Auckland: Australian Geomechanics Society Press, 261–267.
7. Bishop DT, Fityus S (2006) The sensitivity framework: Behaviour of Richmond River estuarine clays, In: Australian Geomechanics Chapter, Sydney Chapter Mini-symposium: Australian Geomechanics Society Press, 167–178.
8. Delage P, Pellerin M (1984) Influence de la lyophilisation sur la structure d'una argile sensible du Quebec. *Clay Miner* 19: 151–160.
9. Li J, Cassidy MJ, Huang J, et al. (2016) Probabilistic identification of soil stratification. *Geotechnique* 66: 16–26.
10. Burland JB (1990) On the compressibility and shear strength of natural clays. *Geotechnique* 40: 329–378.
11. Wood DM (1990) *Soil behaviour and critical strate soil mechanics*. Cambridge University Press.
12. Becker DE, Crooks JHA, Ben K, et al. (1987) Work as a criterion for determining in situ and yield stresses in clays. *Can Geotech J* 24: 549–564.
13. Mesri G, Godlewski PM (1977) Time–stress-compressibility interrelationship. *J Geotech Geoenvironmental Eng* 103: 417–430.
14. Watabe Y, Udaka K, Nakatani Y, et al. (2012) Long-term consolidation behaviour interpreted with isotache concept for worldwide clays. *Soils Found* 52: 449–464.
15. Viggiani G, Atkinson JH (1995) Interpretation of bender elements test. *Geotechnique* 45: 149–154.
16. Jovicic V, Coop MR, Simic M (1996) Objective criteria for determining G_{max} from bender elements tests. *Geotechnique* 46: 357–362.
17. Teh CI, Houlsby GT (1991) An analytical study of the cone penetration test in clay. *Geotechnique* 41: 17–34
18. Leroueil S, Magnan JP, Tavenas F (1990) Embankments on soft clays, *Series in Civil Engineering*. Chichester, UK: Ellis Horwood.

19. Terzaghi K, Peck RB, Mesri G (1996) *Soil Mechanics in Engineering Practice*, 3rd eds. New York, NY, USA: Wiley.

20. Kelly RB, Pineda JA, Bates L, et al. (2018b) Site Characterisation for the Ballina Field Testing Facility. *Géotechnique* 68: 459–462.

21. Won JY (2013) Anisotropic strength ratio and plasticity index of natural clays, *Proceedings 18th International Conference on Soil Mechanics and Geotechnical Engineering*, Paris, France, 445–448.

22. Lunne T, Berre T, Strandvik S (1997) Sample disturbance effects in soft low plasticity Norwegian clay, Symposium on Recent Developments in Soil and Pavement Mechanics, Rio de Janeiro, Balkema, Rotterdam, 81–92.

23. Delage P, Lefebvre G (1984) Study of the structure of a sensitive Champlain clay and of its evolution during consolidation. *Can Geotech J* 21: 21–35.

24. Hight D, Leroueil S (2003) Characterization of soils for engineering purposes. *Charact Eng Prop Nat Soils* 1: 255–362.

25. Lim GT, Pineda J, Boukpeti N, et al. (2019) Effects of sampling disturbance in geotechnical design. *Can Geotech J* 56: 275–289.

26. Kelly RB (2014) Design and construction of a resilient motorway on difficult ground, Proceedings Australian Geomechanics Society, Sydney Chapter Symposium, Australia, 37–45.

27. Doherty JP, Gourvenec S, Gaone FM, et al. (2018) A novel web based application for storing, managing and sharing geotechnical data, illustrated using the national soft soil field testing facility in Ballina, Australia. *Comput Geotech* 93: 3–8.